JOURNAL OF GEOPHYSICAL RESEARCH, VOL. 97, NO. B4, PAGES 5167-5180, APRIL 10, 1992

Geochemical Logging in the Cajon Pass Drill Hole and Its Application to a New, Oxide, Igneous Rock Classification Scheme

ELIZABETH LEWIS PRATSON,[1] ROGER N. ANDERSON,[1] ROY E. DOVE,[2] MITCHELL LYLE,[1] LEON T. SILVER,[3] ERIC W. JAMES,[3,4] AND BRUCE W. CHAPPELL[5]

A new elemental oxide classification scheme for crystalline rocks is developed and applied to geochemical well logs from the Cajon Pass drill hole. This classification scheme takes advantage of measurements of elements taken by a geochemical logging tool string. It uses K_2O versus SiO_2/Al_2O_3 to distinguish between granites, granodiorites, tonalites, syenites, monzonites, diorites, and gabbros. Oxide measurements from cores are used to calibrate the elemental abundances determined from the well logs. From these logs, a detailed lithologic column of the core is generated. The lithologic column derived from the well log classification scheme is compared with a lithologic column constructed from core samples and well cuttings. In the upper 1295 m of the well, agreement between the two columns is good. Discrepancies occur from 1295 to 2073 m and are believed to be caused by the occurrence of rock types not distinguished by the classification scheme and/or the occurrence of secondary minerals. Despite these discrepancies, the well log-based classification scheme helps to distinguish changes in rock type and shows potential as an aid to the construction of lithologic columns in boreholes of crystalline rocks.

INTRODUCTION

The Cajon Pass Scientific Drill Hole is located in the pass between the Los Angeles Basin and the Mojave Desert of California, 32 km (20 miles) northwest of San Bernadino and 3.5 km from the San Andreas fault (Figure 1). The well was drilled as part of the Deep Observation and Sampling of Earth's Continental Crust (DOSECC) program to research deep fault zone properties. The drill hole established an underground laboratory for in situ measurements of the properties near the fault.

One of the main objectives of the Cajon Pass project was addressing the "stress/heat flow paradox." Conventional models derived from fault friction experiments [*Scholz*, 1980] suggest that average shear stress along the San Andreas fault is high (50 MPa). Such high stress should be accompanied by high heat flow. However, none of the approximately 100 shallow heat-flow measurements taken near the San Andreas fault indicates a frictional heat source associated with the fault [*Lachenbruch and Sass*, 1980; *Zoback et al.*, 1980]. Rather, the absence of a heat flow anomaly points to shear stress less than 20 MPa, which implies that frictional coupling across the fault is low [*Lachenbruch, and Sass*, 1988; *Zoback et al.*, 1987]. By drilling a well to seismogenic depths near the San Andreas fault, DOSECC obtained data of both heat flow and stress as a function of depth which could help unravel this paradox.

Since the amounts of heat and stress generated along the fault are dependent on rock type, the lithostratigraphy at the core site must be understood before deciphering the heat flow and stress measurements. Consequently, extensive coring and state-of-the-art logging were combined to allow for continuous measurements of the physical and chemical properties of the rock. Roughly 3 % of the total well depth was cored, of which 85% was recovered. Cutting samples were collected at 3-m (10 foot) intervals and log measurements were taken every 0.15 m (6 inches). Geochemical log measurements help to distinguish lithologic changes and geochemical variations that are not apparent in the geophysical log measurements and that are difficult to pinpoint from cuttings and discontinuous cores. The combination of core data, cutting analysis, and geochemical logs provides the best means for constructing a lithologic column of the strata penetrated by the borehole.

The objectives of this study are twofold. First, we will compare the log-derived elemental and oxide measurements with core-derived oxide measurements and use this relationship of cores to logs to calibrate the geochemical well logs. Second, we will use the calibrated logs to test a new chemical igneous rock classification system which uses the K_2O and SiO_2/Al_2O_3 measurements to differentiate between the major crystalline rock types. The chemical classification scheme can be applied to geochemical analyses from any crystalline rock environment; here it is tested against the Cajon Pass core data and applied to the well logs.

OPERATIONS AT CAJON PASS

The drilling objective of this Cajon Pass project was to reach a total depth of 5 km during three phases of drilling and logging. The first phase of drilling and downhole testing ranged from ground level to 2.12 km. The second phase reached a depth of 3.55 km. The third phase has yet to be drilled; deepening to 5 km is contingent upon the review of all scientific results to date and the availability of future funding. This study will present data obtained during the first and second phases of the project from the basement section of the well (0.7-3.55 km).

[1]Borehole Research Group, Lamont-Doherty Geological Observatory and Department of Geological Sciences, Columbia University, Palisades, New York.
[2]Schlumberger-Doll Research, Ridgefield, Connecticut.
[3]Department of Geological and Planetary Sciences, California Institute of Technology, Pasadena.
[4]Now at Bureau of Economic Geology, University of Texas at Austin.
[5]Department of Geology, Australia National University, Canberra.

Copyright 1992 by the American Geophysical Union.

Paper number 91JB02643.
0148-0227/92/91JB-02643$05.00

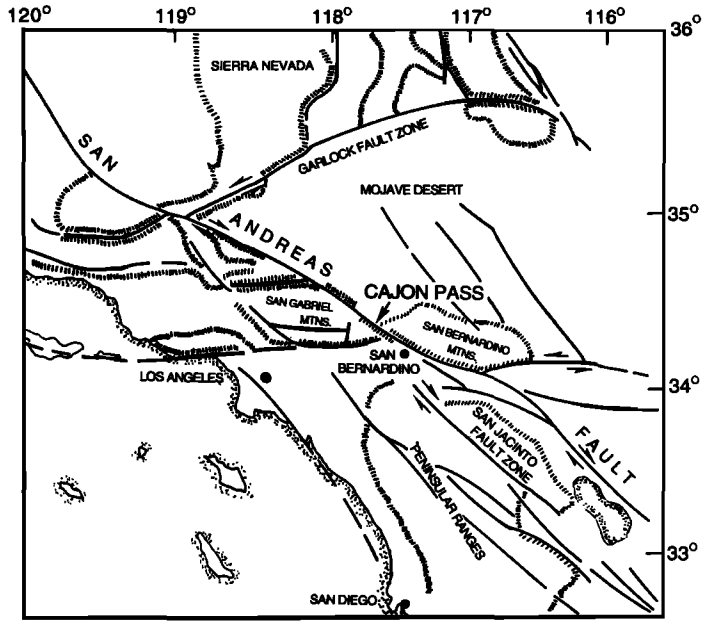

Fig. 1. Location of the Cajon Pass deep drill hole relative to major faults and physiographic features in southern California [*Silver et al.*, 1988].

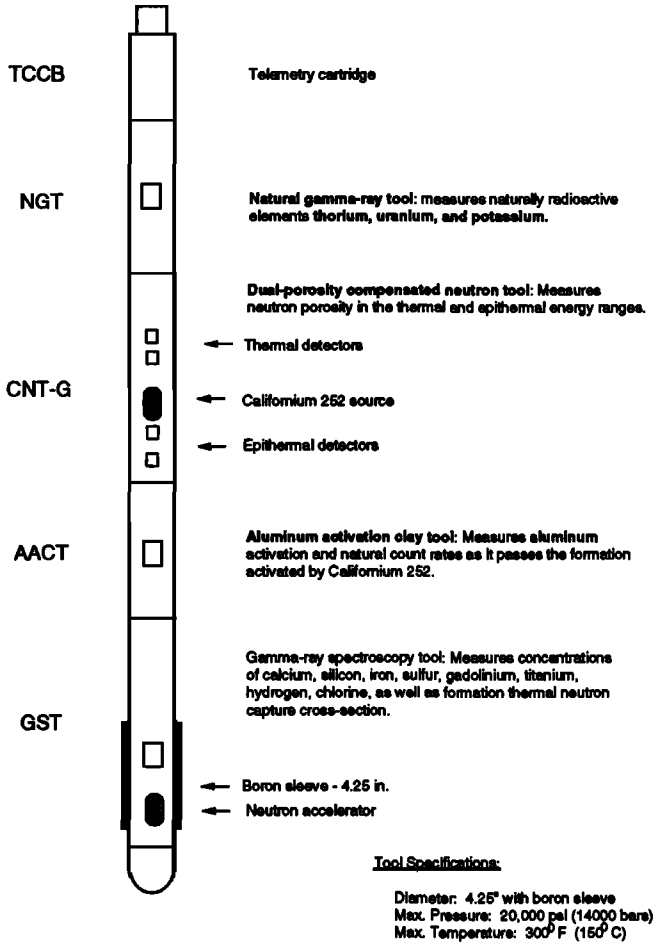

Fig. 2. Schematic drawing of the Geochemical Logging Tool String used by Schlumberger.

An extensive core- and cutting-analysis program was undertaken at the Cajon Pass well. Cuttings were collected every 3 m (10 feet). Fifty spot cores (0.2-8 m, or 0.7-27 feet in thickness) were obtained, and although the cores were taken intermittently, recovery was excellent throughout most of the well. Twenty-two cores were sliced vertically into three slabs, of which the middle slab was powdered and thoroughly mixed for X-ray fluorescence analyses to determine major element abundances.

Logging operations included the recording of electric, acoustic, nuclear, geochemical, and borehole-imaging data. Prior to logging, the upper portion of the well was conditioned with a freshwater, polymer drilling mud system to control viscosity. In the second phase, an NaCl, Mg, Al, silicate-based system was implemented.

GEOCHEMICAL WELL LOGS

Tool Description

The Geochemical Logging Tool string (GLT) consists of four separate logging tools: the natural gamma-ray tool (NGT), the compensated neutron tool (CNT), the aluminum activation clay tool, (ACT), and the gamma-ray spectrometry tool (GST), (GLT, NGT, CNT, AACT, and GST are trademarks of Schlumberger, Figure 2) [*Chapman et al.*, 1987]. The NGT is located at the top of the tool string; therefore, it can measure the naturally occurring radionuclides, Th, U, and K, before the formation is irradiated by the nuclear sources mounted on the trailing tools. The CNT, located below the NGT, carries a low-energy neutron source (^{252}Cf) that activates the Al atoms in the formation. The ACT, a modified NGT, follows, measuring the activated gamma rays in the formation. By combining the ACT measurement with the previous NGT measurement, the background radiation is subtracted out and a reading of formation Al is obtained [*Scott and Smith*, 1973]. The GST, located at the bottom of the string, carries a pulsed-neutron generator to bombard the borehole and formation with high-energy neutrons. A NaI(Tl) scintillation counter measures the spectrum of gamma-rays which are generated. Because the neutron interaction of each of the elements in the formation is characterized by a unique spectral signature, it is possible to derive the contribution (or yield) of the major elements silicon (Si), iron (Fe), calcium (Ca), titanium (Ti), sulfur (S), gadolinium (Gd), and potassium (K) to the measured spectrum and estimate their abundances in the formation. Measurements of hydrogen (H) and chlorine (Cl) in the formation and borehole fluid are also made by the GST.

Well Log Processing

The geochemical well log data obtained in the field were transformed into dry weight percentages of elements and oxides with Schlumberger software at Lamont-Doherty. The processing was as follows: First, borehole corrections were performed on the logs to compensate for the effects of drilling fluids, hole size variations, and logging speed changes. Next, the geochemical log data were transformed into dry weight percentages of the elements while they were normalized with the Al from the ACT and the K from the NGT. The normalization was based upon the assumption that the measured elemental concentrations, recalculated into oxides, form 100% of the rock. This process is explained more fully in previous publications [*Hertzog et al.*, 1987, *Schweitzer et al.*, 1988; *Grau and Schweitzer*, 1989].

Before the GST yields could be normalized, the Ca spectra in

the lower phase of the hole had to be corrected for interference from NaCl in the drilling mud that was used in this section of the hole. Due to the similarity of the spectral signatures of Ca, Na, and Cl, the NaCl mud contaminated the Ca log reading (J. A. Grau. personal communication, 1988.). The Ca yield had to be halved, a is routine process when running the geochemical tool in noncarbonate environments with saline borehole fluids.

The standard oxide factors (multiplication factors used to change elemental concentrations into oxide concentrations) used by Schlumberger in the normalization process are built into the software based on rock types found in typical sedimentary "oil field" environments. At the Borehole Research Group at Lamont-Doherty, in conjunction with Schlumberger-Doll Research, we have altered these oxide factors to represent better the mineralogy encountered in igneous or metamorphic environments. This change is particularly important in the cases of Ca, Fe, and Mg, where the standard Schlumberger software assumes sedimentary carbonate oxide factors of 2.497, 2.075, and 3.472, for $CaCO_3$, $FeCO_3$, and $MgCO_3$ respectively. These oxide factors are explained by *Hertzog et al.*, [1987]). Our revised igneous and metamorphic program assumes oxide factors of 1.399, 1.358, and 1.658, for CaO, FeO*, and MgO respectively (FeO* is the sum total of Fe_2O_3 and FeO, a 50:50 ratio of each is assumed to get the 1.358 oxide factor).

The only major rock-forming elements not measured by the geochemical tool string are magnesium (Mg) and sodium (Na). The neutron-capture cross sections of these elements are too small relative to their typical abundances in the formation to be detected by the GST. Their abundances can, however, be inferred from the photoelectric factor (PEF) measurement from the lithodensity tool. This measured PEF is compared with a PEF calculated from all the measured elements. The PEF is transformed into a dry weight percentage measurement, using a porosity and density curve, before being used to calculate the amount of Mg+Na; this essentially removes the effect of the fluid contribution to PEF. The separation between the measured PEF and the calculated PEF is attributed to unmeasured major elements in the formation, i.e., Mg+Na. Further explanation of this technique is given by *Hertzog et al.* [1987]. Because the PEF is sensitive to changes in hole size and to tool stand-off, the PEF and the Mg+Na calculation is unreliable when hole conditions deteriorate.

If the PEF calculation gives an unreasonably high Mg value, the Schlumberger program calculates Mg based on the assumption that dolomite is the primary mineral containing Mg and assumes the Mg in the dolomite occurs in a constant ratio with Ca. In typical sedimentary "oil field" environments this assumption has been useful but yields erroneous measurements in noncarbonate environments. Because Mg+Na occurs in significant quantities (3-10%) in the Cajon Pass well, we were unable to ignore this calculation if we were to use the logs quantitatively and make any comparison between logs and core measurements.

We implemented a relationship for igneous and metamorphic rocks which bettered the standard Mg calculation based on carbonate lithologies. When the PEF overestimated Mg, Mg was calculated by assuming constant relationship between MgO, FeO*, and SiO_2:

$$FeO^* + MgO = 577.5 \times 10^{(-.0365\ SiO_2)} \quad (1)$$

This relationship was derived by considering the total oxide values of FeO*, SiO_2, and MgO for a broad range of igneous and metamorphic rocks (granites, tonalites, syenites, monzonites, diorites, andesites, gabbros, and dunites) using *Nockolds'*, [1954] data set. This relationship has been used successfully to calculate MgO in other igneous lithologies which were logged with the geochemical tool (e.g., in the Lamont drill hole on the Palisades Sill, where it correctly revealed a Mg-rich olivine layer, and in the Ocean Drilling Program Hole 504B [*Anderson et al.*, 1990]).

GEOCHEMICAL LOGS COMPARED TO AND CALIBRATED WITH CORE MEASUREMENTS

The accuracy of the geochemical logs at Cajon has been tested for the upper 1828 m of the well [*Anderson et al.*, 1990; *Silver, et al.*, 1988], where it was concluded that the logging results were reliable. In this paper we again look at core/log comparisons, but first we scrutinize the depth of each core with respect to the log indicated core depth.

In order to position the cores exactly with respect to the logs, the caliper curve from the Formation MicroScanner logging tool was carefully examined at each cored interval. A unique character was seen on the caliper curve which is best demonstrated in core 50 (Figure 3). An increased hole diameter was noted by C. Williams (personal communication, 1989) at the top and bottom of the cored interval, creating a "mickey-mouse ears" signature. In this example, the depth noted by the driller was 3014.5-3020.6 m (9890-9910 feet), however, the caliper shows that the log depth was 3017.5-3023.7 m (9900-9920 feet), requiring a shift of 3 m (10 feet). The adjustments made to the core depths are listed in Table 1.

The core descriptions were also scrutinized for

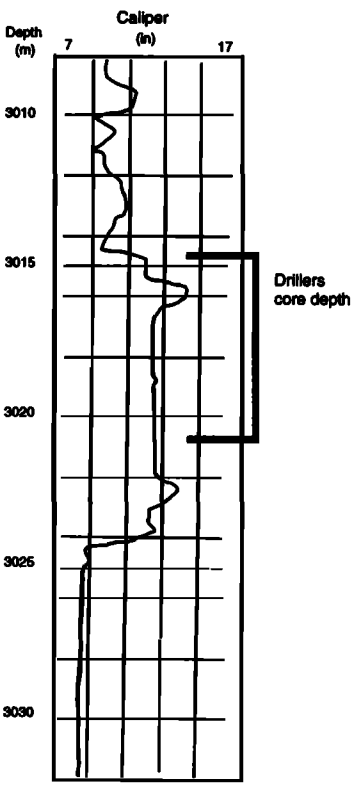

Fig. 3. Demonstration of the caliper curve marking the cored depth intervals, core 50. The coring procedure enlarges the hole at the top and bottom of the interval, indicating a discrepancy between the log and driller's depths of 3 m (10 feet) for this core.

homogeneities of lithology extensive enough to be distinguished by the logs. The core point from core 31, for example, was described as a thin, granitic-to-granodioritic layer which had been injected into an amphibole. The granodiorite sampled was too thin to be seen on the logs; therefore, this sample was not used in the core-log comparison. Other cores (6 and 52) were not used either because their sampling intervals were less than 0.15 m (6 inches).

Prior to the comparison, a 10-point smoothing filter had been applied to the logs to remove some of the noise. In order to obtain a measurement that would be comparable with core values, the log values were again averaged within the core-sampled interval. A list of the core and log values is given in Table 2.

Separate comparisons are made for the upper and lower sections of the Cajon Pass well, because different fluids were added to the hole during each logging pass: fresh water in the upper phase and NaCl/gel in the lower phase. It was necessary to see whether the different fluids had any adverse affect on any of the measured elements other than Ca.

Cross plots of core versus log data, along with linear regression analyses of core measurements versus logs are displayed in Figure 4 for phases I and II. Terminology for reliability of the linear regression lines follows: $R \geq 0.75$ is good; $R < 0.75$ but > 0.5 is fair; and $R \leq 0.5$ is poor. SiO_2, FeO*, and K_2O display a good relationship in both the upper and lower phases of drilling. Al_2O_3, CaO, and TiO_2 show a fair (CaO) to good (Al_2O_3 and TiO_2) relationship in phase I but a poor one in phase II. It is likely that the clays which were added to the borehole to control viscosity in the lower portion of the well (AQUAGEL, a bentonite, Na-montmorillonite mud; SEA MUD, a sepiolite, hydrated Mg silicate mud; ZEOGEL, a Mg-Al-silicate; and BARAZAN, a polymer) interfered with these elements, causing the Al_2O_3 measurement to be too high in Phase II, especially in zones of hole washout. NaCl also interferes with the elemental yields, especially in zones of washout, despite corrections applied to the Ca yield. It is also possible that there are trace amounts of Ti in the drilling muds or that there is interference induced into the Ti yield by an element in the drilling fluids with a similar spectral signature. The MgO + Na_2O measurement is good in phase II, but is poor in phase I.

After having compared log and core values, we use a linear regression to calibrate the logs and so account for uniform tool error or incorrect assumptions in our oxide calculation method. Where the line fit is good ($R \geq 0.75$), the linear regression coefficients are used to force a 1:1 relationship between the log and core values. The calibrated logs are displayed with core points for comparison in Figure 5.

TABLE 1. Depth Corrections Applied to Core Depths

Core	Core Cut, m	Recovered/ Drilled Core, m	Caliper Indicated Core Depth, m	Shift, m	Sampled Core Interval, m	Log Interval used in Correlation, m
5	521.18-529.44	8.23/8.23	520.60-528.83	-0.61	525.57-525.73	524.87-525.18
6	594.33-596.81	?/2.44	undetermined	-0.61	594.95-595.01	594.37
10	743.37-746.16	2.59/2.74	743.42-746.16	-0.91	744.45-744.94	743.57-744.03
15	1138.07-1141.19	2.80/3.05	1138.14-1141.19	-0.91	1138.99-1140.27	1138.99-1139.36
17	1350.81-1356.68	5.43/5.79	flat caliper	0	1352.87-1353.33	1352.87-1353.33
18	1499.54-1501.16	1.74/1.74	1499.63-1501.37	-0.91	1500.70-1501.37	1499.79-1500.4
19	1651.63-1657.83	5.94/6.10	flat caliper	0	1655.63-1657.31	same
20	1740.93-1744.09	2.82/3.05	undetermined	-0.91	1741.07-1741.37	1740.12-1740.43
21	1843.95-1845.28	1.07/1.22	1844.67-1845.89	0.61	1844.98-1845.28	1845.59-1845.89
28	1981.71-1984.27	1.89/2.44	1979.70-1982.44	1.98	1982.87-1983.21	1980.92-1981.22
30	2042.06-2045.53	2.68/3.35	2039.14-2042.49	-3.05	2043.40-2043.71	2040.36-2040.66
33	2076.50-2079.66	2.83/3.05	2075.10-2078.15	-1.52	2077.85-2077.94	2076.32-2076.48
35	2182.26-2191.54	6.40/9.14	flat caliper	0	2186.48-2186.81	2186.51-2186.81
36	2246.27-2250.06	3.66/3.66	on depth	0	2247.32-2248.22	2247.32-2248.23
37	2286.50-2289.69	2.83/3.05	2285.42-2288.47	-1.22	2287.70-2288.16	2286.49-2286.94
39	24256.94-2431.33	5.70/5.70	on depth	0	2429.07-2430.38	2429.13-2286.94
42	2603.78-2604.85	0.67/1.13	on depth	0	2604.18-2604.58	2604.24-2604.55
46	2741.54-2747.20	5.40/5.49	2740.19-2745.67	-1.52	2746.13-2747.10	2744.60-2745.37
49	2886.32-2889.08	1.80/2.59	2889.23-2891.67	2.74	2887.53-2888.02	2890.27-2890.76
50	3014.32-3020.60	4.88/6.10	3017.56-3023.65	3.05	3018.35-3018.90	3021.37-3021.98
52	3343.49-3348.88	0.70/5.18	3345.22-3350.40	1.52	3344.28-3344.35	3345.80-3345.98

TABLE 2. Core Versus Oxide Measurements

Core	Depth, m	SiO_2 Core	SiO_2 Log	TiO_2 Core	TiO_2 Log	Al_2O_3 Core	Al_2O_3 Log	FeO* Core	FeO* Log	MgO+ Na_2O Core	MgO+ Na_2O Log	CaO Core	CaO Log	K_2O Core	K_2O Log
C-5	525.02	65.37	69.35	0.63	0.84	15.66	12.97	3.26	4.23	5.20	2.48	3.13	6.50	3.19	3.63
	525.18		69.08		0.85		12.94		4.18		2.64		6.65		3.59
			69.21		0.85		12.96		4.21		2.56		6.58		3.61
C-6	594.37	71.57	72.56	0.34	0.23	14.45	18.34	1.85	0.84	3.95	0	2.03	3.51	5.05	4.51
			72.56		0.23		18.34		0.84		0		3.51		4.51

TABLE 2. (continued)

Core	Depth, m	SiO_2 Core	SiO_2 Log	TiO_2 Core	TiO_2 Log	Al_2O_3 Core	Al_2O_3 Log	FeO* Core	FeO* Log	MgO+ Na_2O Core	MgO+ Na_2O Log	CaO Core	CaO Log	K_2O Core	K_2O Log
C-10	743.57	73.06	73.67	0.32	0.13	13.68	14.66	1.73	0.90	3.98	2.37	1.79	4.23	4.45	3.78
	743.72		73.91		0.12		14.98		0.88		1.95		4.21		3.77
	743.87		74.44		0.11		15.07		0.90		1.50		4.09		3.75
	744.03		75.95		0.1		14.91		0.96		0.47		3.81		3.70
			74.49		0.12		14.91		0.91		1.57		4.09		3.75
C-15	1137.98	71.02	67.50	0.46	0.41	13.79	17.28	3.05	2.80	3.69	4.74	1.88	4.36	4.81	3.41
	1138.14		67.77		0.40		17.00		2.33		4.23		4.77		3.44
	1138.29		67.41		0.39		16.98		2.32		4.16		5.21		3.48
	1138.44		68.35		0.39		16.95		2.35		2.99		5.30		3.53
	1138.59		69.03		0.39		16.89		2.38		2.26		5.28		3.65
	1138.75		68.85		0.39		16.79		2.36		2.30		5.43		3.77
	1138.90		68.66		0.39		16.52		2.34		2.62		5.52		3.88
	1139.05		68.39		0.38		16.58		2.28		3.22		5.11		3.96
	1139.20		67.64		0.4		16.58		2.21		3.88		5.15		4.03
	1139.36		66.78		0.43		16.77		2.11		4.46		5.23		4.14
			68.04		0.40		16.83		2.35		3.49		5.14		3.73
C-17	1352.72	61.52	64.09	0.88	1.09	17.05	20.33	4.33	3.36	5.31	3.95	4.73	6.07	2.38	2.37
	1352.87		62.04		1.10		20.43		3.30		4.39		6.88		2.35
	1353.02		60.88		1.11		20.31		3.33		4.31		7.26		2.35
	1353.18		62.04		1.11		20.15		3.43		3.56		6.88		2.36
	1353.33		64.09		1.11		20.25		3.59		2.05		6.07		2.38
			62.63		1.10		20.29		3.40		3.65		6.63		2.36
C-18	1499.79	61.01	70.02	1.07	0.83	14.94	14.55	6.74	4.82	5.19	2.90	3.47	3.31	3.44	3.20
	1499.94		69.57		0.87		14.59		5.05		2.89		3.47		3.21
	1500.09		68.85		0.90		14.67		5.27		2.97		3.95		3.23
	1500.24		67.74		0.93		14.59		5.45		3.08		4.76		3.28
	1500.40		67.01		0.96		14.55		5.64		3.05		5.28		3.34
			68.64		0.90		14.59		5.24		2.98		4.15		3.25
C-19	1655.69	67.11	66.61	0.56	0.70	15.58	17.10	3.12	2.43	7.38	3.75	3.24	6.28	4.29	4.13
	1655.85		66.53		0.70		16.93		2.44		3.27		5.92		4.22
	1656.00		67.19		0.70		17.02		2.39		2.73		5.71		4.26
	1656.15		68.79		0.68		16.86		2.41		1.74		5.27		4.25
	1656.30		70.37		0.66		16.97		2.38		0.92		4.50		4.20
	1656.46		70.98		0.65		17.16		2.30		0.81		4.01		4.13
	1656.61		70.99		0.63		17.35		2.20		1.06		3.74		4.03
	1656.76		71.16		0.61		17.32		2.14		0.97		3.71		3.97
	1656.91		71.07		0.59		17.37		2.08		1.36		3.38		3.91
	1657.07		70.52		0.57		17.52		2.00		1.76		3.40		3.88
	1657.22		69.98		0.54		17.87		1.91		2.04		3.40		3.82
	1657.37		69.74		0.52		18.22		1.81		1.69		3.76		3.77
			69.49		0.63		17.31		2.21		1.84		4.42		4.05
C-20	1740.12	43.85	60.00	1.30	0.85	18.48	19.54	11.25	4.83	4.10	4.42	11.54	7.64	0.89	2.44
	1740.28		58.23		0.93		19.49		5.61		4.89		8.20		2.20
	1740.43		55.85		1.00		19.28		6.32		5.77		9.22		1.99
			58.03		0.92		19.44		5.59		5.02		8.35		2.21
C-21	1845.59	55.61	54.79	1.12	0.85	17.74	17.35	6.60	6.46	8.37	6.18	6.39	11.68	2.02	2.69
	1845.74		54.05		0.90		17.36		6.74		6.31		12.01		2.63
	1845.89		53.48		0.95		17.31		7.01		6.40		12.30		2.55
			54.11		0.90		17.34		6.73		6.29		12.00		2.62
C-28	1980.92	66.72	55.15	0.49	0.71	16.60	23.91	2.39	2.42	6.10	7.49	2.75	6.54	3.22	3.78
	1981.07		55.00		0.78		23.93		2.41		7.51		6.34		4.03
	1981.22		54.94		0.84		23.87		2.43		7.50		6.14		4.28
			55.03		0.78		23.90		2.42		7.50		6.34		4.03
C-30	2040.36	54.86	58.27	1.43	1.30	16.98	17.81	7.47	6.93	7.62	5.47	6.73	7.50	2.10	4.88
	2040.51		58.33		1.33		17.84		7.04		5.28		7.57		4.90
	2040.66		58.27		1.35		17.79		7.15		5.07		7.70		4.90
			58.29		1.32		17.81		7.04		5.27		7.59		4.90

TABLE 2. (continued)

Core	Depth, m	SiO_2 Core	SiO_2 Log	TiO_2 Core	TiO_2 Log	Al_2O_3 Core	Al_2O_3 Log	FeO* Core	FeO* Log	MgO+ Na_2O Core	MgO+ Na_2O Log	CaO Core	CaO Log	K_2O Core	K_2O Log
C-33	2076.32	57.27	55.97	0.95	1.21	16.15	17.94	7.14	8.00	5.34	5.13	6.59	9.11	2.04	2.63
	2076.48		56.15		1.24		17.92		7.97		5.31		8.82		2.59
			56.06		1.22		17.93		7.99		5.22		8.96		2.61
C-35	2186.51	61.27	68.85	0.47	0.66	18.20	18.26	3.31	3.01	5.34	0.57	3.94	3.76	5.19	4.88
	2186.66		69.26		0.70		18.25		2.90		0.48		3.50		4.90
	2186.81		69.48		0.73		18.25		2.81		0.45		3.37		4.90
			69.20		0.70		18.25		2.91		0.50		3.54		4.90
C-36	2247.32	53.83	54.91	1.00	1.08	14.81	19.26	9.45	7.79	8.11	7.56	7.68	7.40	1.71	2.07
	2247.47		54.93		1.10		19.52		7.90		7.55		7.49		1.94
	2247.62		54.86		1.15		19.03		8.05		7.54		7.57		1.85
	2247.77		54.70		1.18		18.91		8.23		7.53		7.67		1.81
	2247.93		54.48		1.20		18.80		8.41		7.51		7.80		1.80
	2248.08		54.23		1.21		18.71		8.57		7.50		7.92		1.82
	2248.23		54.02		1.21		18.60		8.68		7.48		8.04		1.88
			54.59		1.16		18.98		8.23		7.52		7.70		1.88
C-37	2286.49	67.98	63.78	0.54	1.29	15.09	16.56	2.96	4.34	4.63	4.64	2.75	5.39	4.43	4.06
	2286.64		64.28		1.30		16.21		4.38		4.59		5.22		4.06
	2286.79		64.73		1.31		15.84		4.40		4.54		5.14		4.07
	2286.94		65.17		1.30		15.45		4.41		4.50		5.10		4.08
			64.49		1.30		16.01		4.38		4.57		5.21		4.07
C-39	2429.13	61.63	64.36	0.77	1.34	16.79	12.96	5.03	6.42	5.94	5.11	4.96	7.14	3.03	2.66
	2429.29		64.21		1.35		12.61		6.59		5.18		7.46		2.61
	2429.44		64.04		1.36		12.24		6.78		5.27		7.75		2.56
	2429.59		63.91		1.37		11.89		6.99		5.40		7.97		2.51
	2429.74		63.82		1.38		11.60		7.19		5.45		8.08		2.48
	2429.90		63.77		1.40		11.36		7.38		5.53		8.10		2.46
	2430.05		63.74		1.42		11.16		7.58		5.61		8.03		2.46
	2430.20		63.71		1.45		10.99		7.79		5.70		7.88		2.47
	2430.35		63.66		1.51		10.88		7.99		5.79		7.70		2.48
			63.91		1.40		11.74		7.19		5.45		7.79		2.52
C-42	2604.24	67.90	64.04	0.48	0.91	15.61	19.44	3.32	4.19	4.78	2.32	3.36	5.55	3.92	3.55
	2604.40		64.11		0.92		19.41		4.19		2.15		5.49		3.69
	2604.55		64.26		0.92		19.36		4.19		1.98		5.48		3.81
			64.13		0.92		19.40		4.19		2.15		5.51		3.68
C-46	2744.60	60.02	65.09	0.78	0.83	17.39	17.50	5.67	4.81	6.46	2.82	5.67	5.89	2.45	3.06
	2744.76		65.43		0.87		17.24		4.90		2.88		5.63		3.06
	2744.91		65.70		0.91		17.00		5.02		2.93		5.44		2.99
	2745.06		65.89		0.96		16.82		5.16		3.00		5.26		2.92
	2745.21		65.99		1.01		16.68		5.31		3.07		5.08		2.85
	2745.37		66.04		1.06		16.60		5.47		3.14		4.92		2.78
	2745.52		66.03		1.09		16.56		5.61		3.22		4.78		2.70
			65.74		0.96		16.91		5.18		3.01		5.29		2.91
C-49	2890.30	71.10	75.61	0.18	0.61	14.04	15.32	1.37	1.65	3.96	0.31	2.04	2.26	4.30	4.24
	2890.45		75.58		0.58		15.47		1.65		0.30		2.17		4.25
	2890.61		75.49		0.57		15.46		1.69		0.27		2.07		4.26
	2890.76		75.31		0.59		15.81		1.76		0.28		1.96		4.29
			75.50		0.59		15.52		1.69		0.29		2.12		4.26
C-50	3021.37	63.01	62.35	0.66	1.63	15.82	19.17	4.62	5.01	5.70	4.09	4.70	3.69	3.18	4.05
	3021.52		62.12		1.55		19.15		5.04		4.16		3.98		4.01
	3021.67		61.95		1.45		19.19		5.00		4.20		4.22		3.98
	3021.82		61.80		1.34		19.32		4.92		4.23		4.42		3.97
	3021.98		61.65		1.23		19.55		4.79		4.25		4.57		3.96
			61.97		1.44		19.28		4.95		4.19		4.18		3.99
C-52	3345.83	73.84	72.16	0.29	1.28	12.62	18.41	2.52	3.30	3.10	1.11	1.84	1.06	4.89	4.19
	3345.98		71.62		1.34		19.02		3.25		1.22		1.02		4.23
			71.89		1.31		18.72		3.28		1.17		1.04		4.21

Bottom log value is the averaged log value over the interval. This averaged value was used in the log-core comparison.

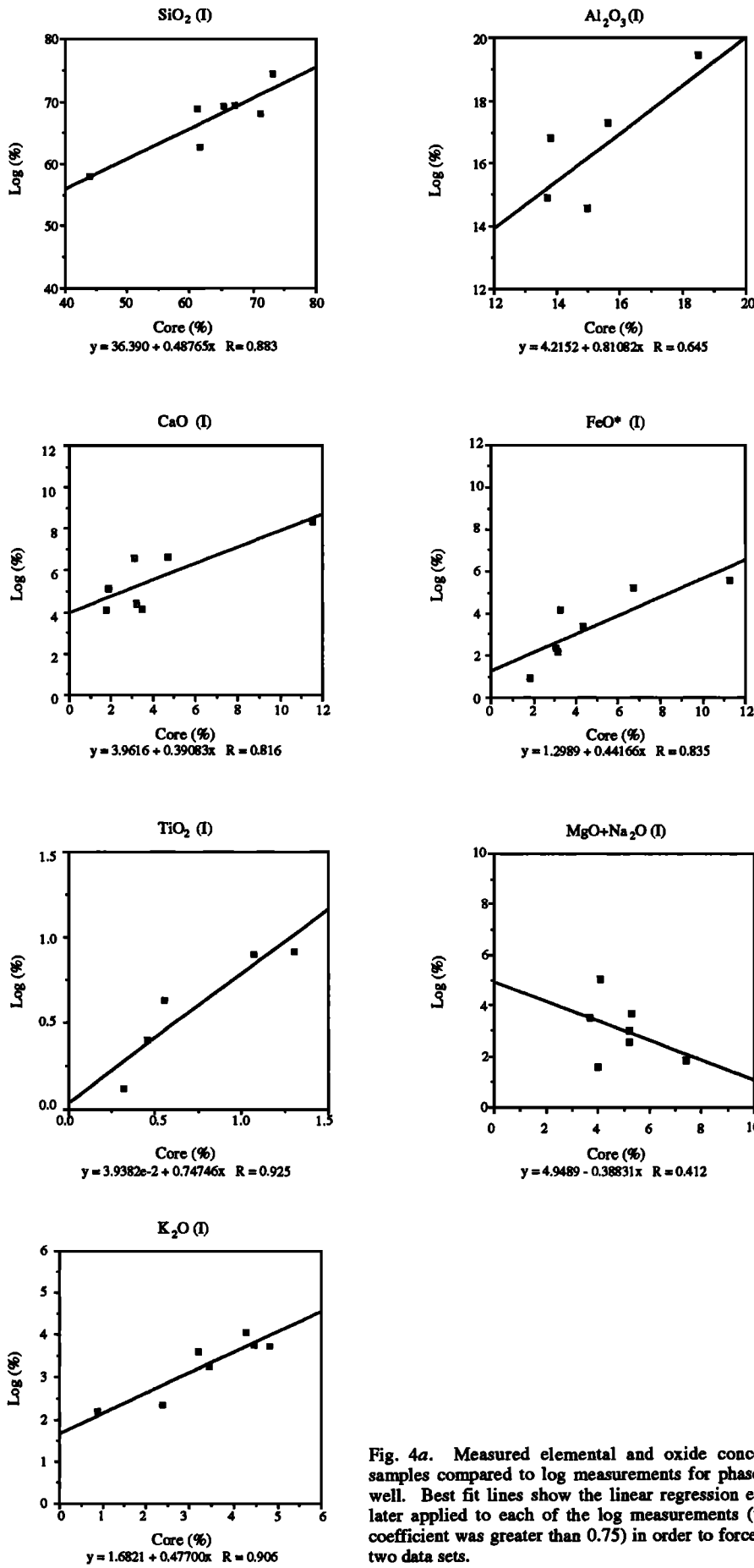

Fig. 4*a*. Measured elemental and oxide concentrations from core samples compared to log measurements for phase I of the Cajon Pass well. Best fit lines show the linear regression equations, which were later applied to each of the log measurements (where the correlation coefficient was greater than 0.75) in order to force a 1:1 fit between the two data sets.

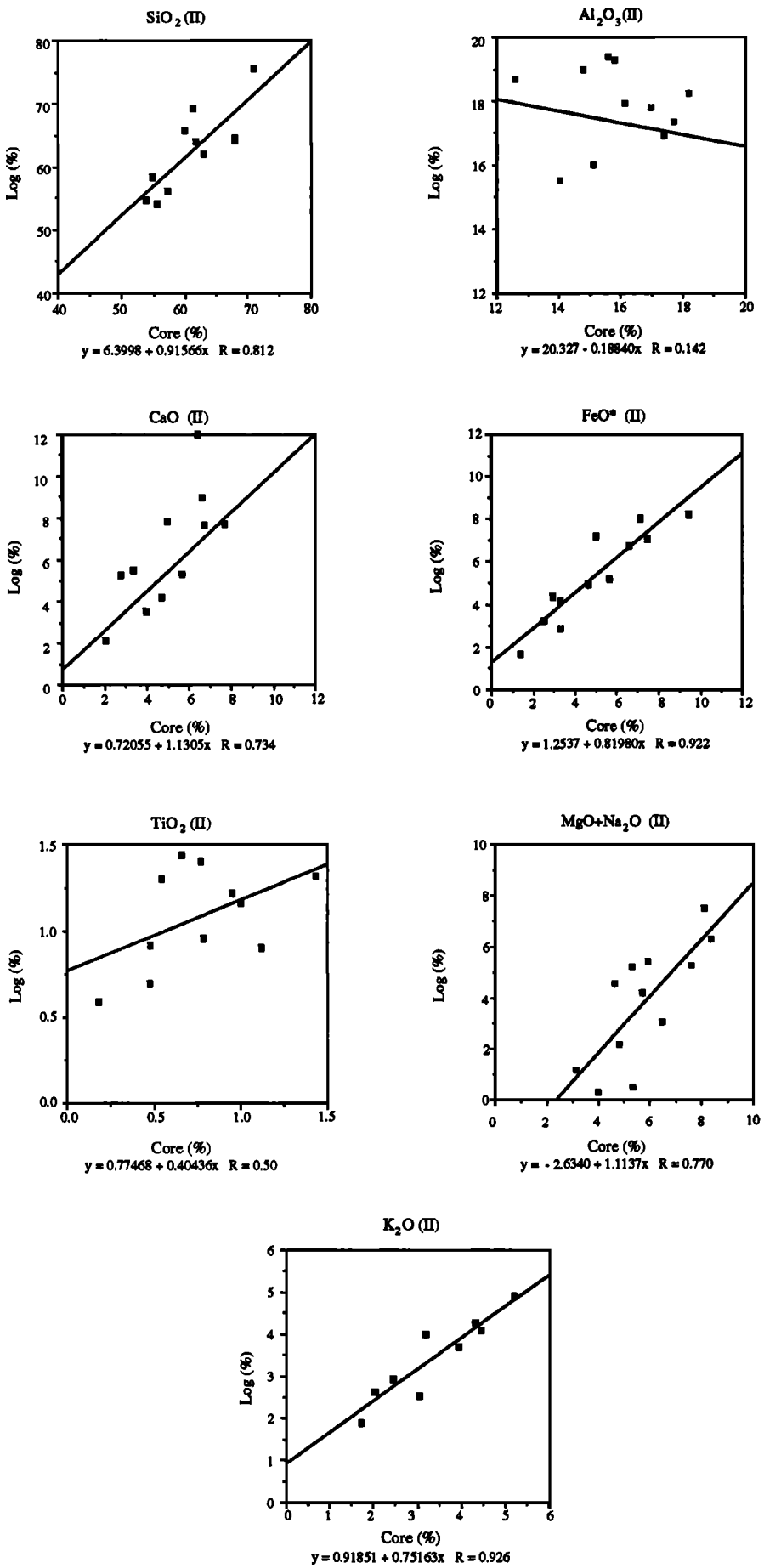

Fig. 4*b*. Same as Figure 4*a* , except it is phase II.

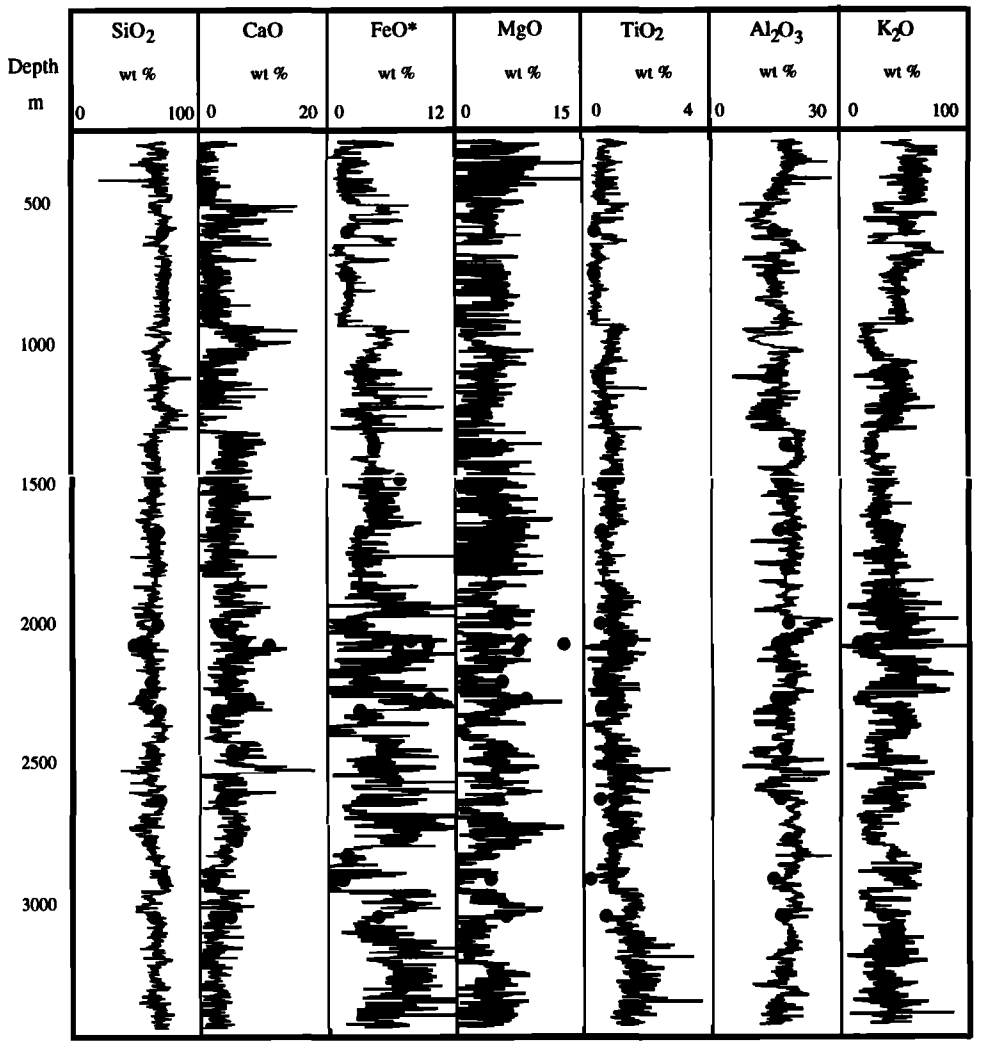

Fig. 5. Final oxide results from log measurements compared to XRF core measurements after logs were calibrated to core.

APPLICATION OF GEOCHEMICAL MEASUREMENTS

As it is difficult to define directly the lithology from oxide or elemental measurements, well log data are often transformed into mineral abundances [*Flaum and Pirie*, 1981; *Peveraro and Russell*, 1984; *Herron*, 1986; *Anderson et. al.*; 1988 *Wendlandt and Bhuyan*, 1990]. This transformation is done using a matrix-inversion method that simultaneously solves a set of linear log response equations, a method which is explained in more detail by *Doveton* [1986]. These mineral percentage logs, although useful when contrasted with point count analyses, still do not directly compare to lithologic

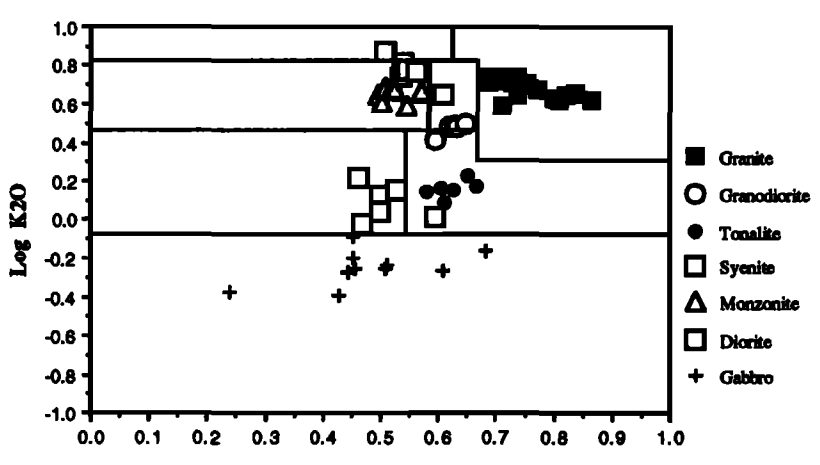

Fig. 6. The IgClass system which uses geochemical measurements to distinguish major crystalline rock types.

TABLE 3. Field Boundary Definitions for the IgClass System

Lithologic Field	Log K_2O	Log SiO_2/Al_2O_3
Granite	0.8 to 1.0	0.625 to 1.0
	0.3 to 0.8	0.675 to 1.0
Granodiorite	0.47 to 0.8	0.54 to 0.675
Tonalite	0.085 to 0.47	0.5 to 0.675
	-0.085 to 0.3	0.675 to 1.0
Syenite	0.8 to 1.0	0.3 to 0.58
Monzonite	0.47 to 0.8	0.3 to 0.58
Diorite	-0.085 to 0.47	0.3 to 0.54
Basalt	-0.7 to -0.85	0.0 to 1.0

descriptions made through visual classification of cores.

Classification schemes which directly use chemical measurements have been devised for sedimentary rock types [*Middleton*, 1960; *Pettijohn et al.* 1972; *Herron*, 1988]. Herron derived a geochemical classification for terrigenous rocks using the primary parameters of SiO_2/Al_2O_3 and Fe_2O_3/K_2O, and $CaCO_3$ as a secondary parameter. This classification scheme, named "SandClass," was successfully tested on both core and geochemical well log measurements and is now routinely used to classify rock types when logging with the geochemical tool in sedimentary environments.

We introduce an "IgClass" scheme similar to Herron's SandClass, which directly transforms oxide measurements into crystalline rock types. The major igneous rock types

a

Quartz & Other Minerals	Potash feldspar relative to total feldspar content					
	Kspar 100-60%	Kspar >60%	Kspar 60-40%	Kspar 40-10%	Kspar <10%	No Kspar
Qtz. >10%	GRANITE (Rhyolite)	CALC-ALK GRANITE (Calc-alk Rhyolite)	ADAMELLITE (Dellenite)	GRANO-DIORITE (Rhyo-dacite)	TONALITE (Dacite)	
No Qtz. or Feldspathoid (i.e. <10%)	SYENITE (Trachyte)	CALC-ALK SYENITE (Calc-alk Trachyte)	MONZONITE (Latite)	MANGERITE (Dorute)	DIORITE (Andesite) GABBRO (Basalt)	PERKNITE PERIDOTITE
Feldspathoid >10%	NEPHALINE SYENITE (Phonolite)		NEPHELINE MONZONITE (Nepheline latite)	ESSEXITE (Nepheline ordanchite) GLENMU-IRITE (Analcite ordanchite)	THERALITE (Nepheline tephrite) TESCHENITE (Analcite tephrite)	ULTRA-ALKALINE ROCKS (Nephelinite, etc.)

(after Nockolds, 1954)

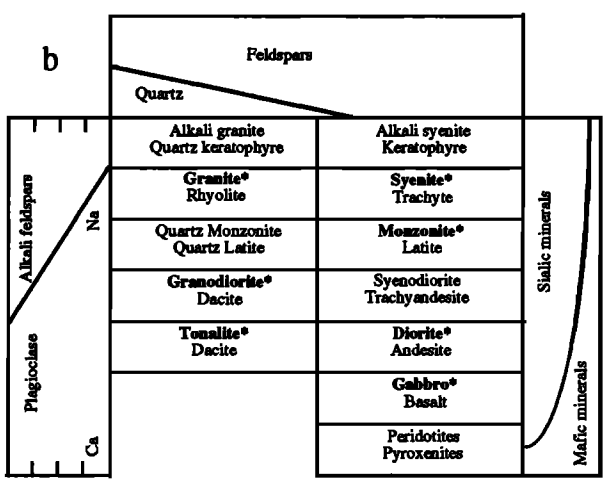

(after Jackson, 1970)

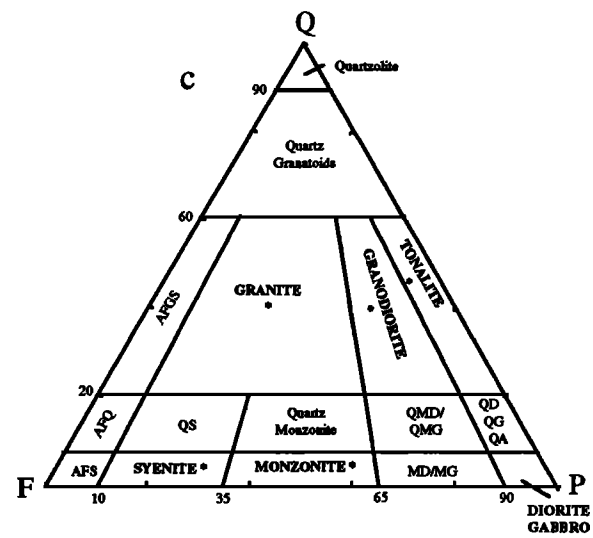

(after Streckeisen, 1976)

Fig. 7. Comparison of igneous and metamorphic rock classification schemes of: (*a*) *Nockolds*, [1954], (*b*) *Streckeisen*, [1976], and (*c*) *Jackson*, [1970]. Nockolds' classification scheme, although much older than the scheme used at Cajon *[Streckeisen*, 1976] to classify cores and cuttings, agrees well for the major rock types solved for in the IgClass system. Like Nockolds, the Streckeisen diagram bases rock distinction on quartz content and on the ratio of potash to plagioclase feldspar content. Jackson's scheme is based on the ratio of quartz to feldspars, the types of feldspars present, and mafic mineral content. Overall, the three schemes agree within 10% in quartz and feldspar content.

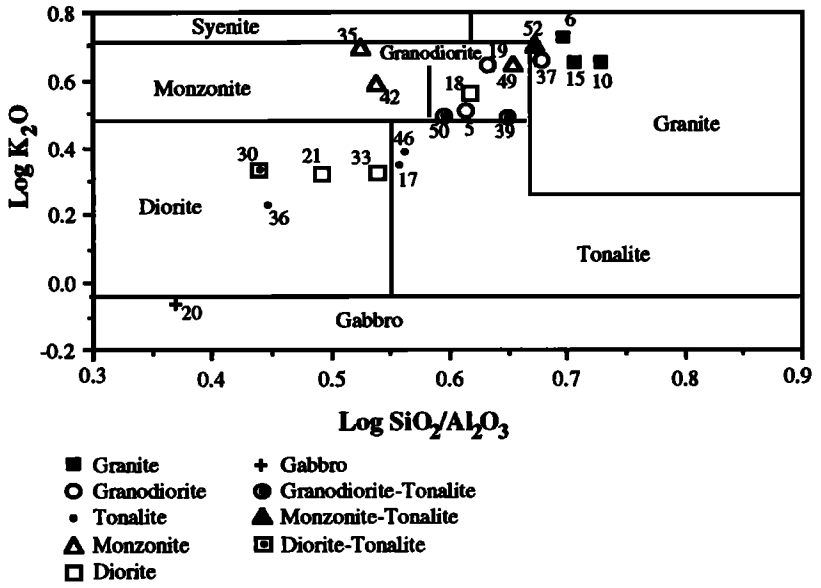

Fig. 8. Cajon Pass core data incorporated into the IgClass system. Numbers refer to core numbers, listed in Table 4.

were discerned using *Nockolds'* [1954] large compilation of measurements which includes average chemical compositions for common igneous and metamorphic rock types. From this data set, discriminate analysis determined that the cross plot of K_2O versus SiO_2/Al_2O_3 best distinguishes the major rock types of granite, granodiorite, tonalite, syenite, monzonite, diorite, and gabbro. Figure 6 displays the rock-type fields defined by these oxides (field boundaries are defined in Table 3).

Because the classification scheme is based on chemical rock variations only, it does not incorporate textural features. Nor does the IgClass system distinguish between coarse-grained (porphyritic) and fine-grained (aphanitic) rock types. The coarse-grained version of each chemical rock type is displayed in the IgClass chart; however, we are essentially combining the fine-grained and coarse-grained textural rock types into one (for instance, both basalts and gabbros will be called gabbros and both granites and rhyolites will be classified as granites with the IgClass scheme).

In the context of mineral classification schemes, the decision to use these three oxides becomes clear. Figure 7 displays the mineral classification schemes of *Jackson* [1970], *Nockolds* [1954], and *Streckeisen* [1976]. In each of these classification schemes potassium feldspar (seen as potash feldspar by Nockolds, alkali feldspar by Jackson, and K by Streckeisen) is used as an end-member to classify the

TABLE 4. Cajon XRF Applied to IgClass and Comparison of Lithologic Description

Core	Log (SiO_2/Al_2O_3)	Log (K_2O)	Lithologic Description	IgClass Calassification
C-5	0.61	0.50	Sphene hornblende biotite granodiorite	Granodiorite
C-6	0.69	0.70	Sphene-biotite granite	Granite
C-10	0.73	0.65	Allanite-sphene biotite granite	Granite
C-15	0.71	0.68	Migmatic granitic gneiss	Granite
C-17	0.56	0.38	Sphene hornblende-biotite tonalite	Tonalite
C-18	0.61	0.54	Migmatic hornblende biotite diorite to quartzofeldspathic gneiss	Granodiorite
C-19	0.63	0.63	Granodiorite	Granodiorite
C-20	0.38	-0.05	Hornblende gabbro	Gabbro
C-21	0.50	0.31	Migmatic sphene horneblende-biotite diorite to granodiorite biotite	Diorite
C-30	0.44	0.32	Heterogeneous diorite to quartz diorite	Diorite
C-33	0.54	0.31	Heterogeneous diorite to quartz diorite	Diorite
C-35	0.53	0.72	Biotite-hornblende quartz monzodiorite	Monzonite
C-36	0.45	0.23	Interlayered quartz-biotite amphibolite and mafic biotite-hornblende. tonalite gneiss	Diorite
C-37	0.68	0.65	Sphene-hornblende biotite granodidorite gneiss	Granodiorite/granite
C-39	0.65	0.48	Homogeneous hornblende-biotite granodiorite/tonalite	Granodiorite/tonalite
C-42	0.54	0.59	Sphene biotite monzogranite gneiss	Monzonite
C-46	0.56	0.39	Biotite-hornblende tonalite gneiss	Tonalite
C-49	0.66	0.63	Well foliated biotite monzogranite gneiss	Granodiorite
C-50	0.60	0.50	Biotite-hornblende granodiorite to tonalite gneiss	Granodiorite/tonalite
C-52	0.68	0.69	Biotite monzogranite tonalite gneiss	Granodiorite/granite

rocks. Similarly, the K_2O content in the IgClass system reflects the potassium feldspar content of the rock. In each of the classification schemes, syenites and granites are rich in potassium feldspars, whereas monzonites and granodiorites are composed of intermediate amounts of alkali feldspar and plagioclase feldspar, and diorites, tonalites, and gabbros are dominantly composed of plagioclase feldspar. Quartz is also used by each of the three classification schemes shown in Figure 7 (represented by Q by Streckeisen). Likewise, the SiO_2/Al_2O_3 axis in the IgClass system relates to the quartz content of the rock. Granites, granodiorites, and tonalites, which are rich in quartz (>10%), are compared to the low quartz content of syenites monzonites, diorites, and gabbros. Unlike the SandClass system, iron oxide is not used to distinguish rock types, as its inclusion was found to decrease the field boundary resolution in the IgClass system.

IgClass Applied to Cores

Before incorporating the oxide classification scheme to logs, 20 of the representative Cajon core measurements are integrated into the IgClass system (Figure 8 and Table 4) This classification system correctly classifies all but four of the 20 cores (cores 18, 36, 49, and 52). Discrepancies occur when the lithologies are either very heterogenous or contain significant secondary alteration and accessory minerals to alter the overall rock chemistry.

The majority of the cores were correctly classified in terms of overall rock type. We can see from Table 4 that IgClass is not able to include textural descriptions or provide information of secondary minerals as visual core description can. IgClass does, however, classify major rock types successfully when the rocks are fairly uniform in lithology and do not contain secondary minerals.

IgClass Applied to Well Logs

As well logs provide continuous measurements of the oxides in the rock, including those that support the IgClass system, we can apply the system to the Cajon Pass geochemical well log measurements. The wide range in rock types encountered at this well provides an excellent locale for testing the IgClass system.

The Schlumberger "LITHOS" program, a program used for statistically determining and solving for electrofacies, was altered to incorporate our IgClass system with input logs of K_2O and SiO_2/Al_2O_3. The results of IgClass incorporated into Cajon Pass logs (Plate 1) are compared to a lithologic description which was prepared by L. Silver, E. James, and S.Cotkin through extensive examination and thin section studies of both cores and cuttings. The IUGS petrographic nomenclature of *Streckeisen* [1976] was used by Silver et al. to classify the Cajon Pass rocks. The IgClass results identifies the complex nature and variety of rock-types found at Cajon Pass unraveled by traditional methods.

The lithologic column consists of 16 units derived from the combined log classification and core/cutting descriptions. The two data sets correlate reasonably well in terms of lithologic classification, but the local depths of the major lithologic changes do not match. The unit depths used in this paper refer to the log depths, which we feel are more reliable than depths based on cuttings or intermittent cores.

The upper five units (500-1298 m) are classified by the logs as primarily granites and granodiorites; this agrees well with the description from cores/cuttings. A fault marks the lower boundary of unit 5, which is depicted on the log-based lithologic column by a distinct color change.

The log-based and core-based lithologic columns indicate unit 6 (1298-1438 m) differently: the log-based column shows a diorite-to-tonalite lithology, and the core-based shows a granodiorite lithology. The presence of mafic minerals (sphene, hornblende, and biotite) are responsible for this discrepancy.

Unit 7 (1438-1658 m), seen on the log-based column as a highly variable section, grades from granodioritic and tonalitic to dioritic units. The rocks of unit 8 (1658-1747 m) are described as migmatitic quartzo feldspathic gneiss. This is one example where IgClass cannot classify this rock type because it is primarily a textural classification and IgClass uses chemical information as its input. A distinct bed of gabbro did show up on the enlarged scale of the IgClass log at 1737 m (not discernable, however, at this scale) which corresponds to the hornblende gabbro sheet described in core in this same interval. Unit 9 (1747-1839 m) is classified as a granodiorite.

The log- and core-based columns at first seem to disagree in their depiction of unit 10. Granodiorites and quartz diorites are described in the rocks, but monzonites dominate the log-based column. Because diorites and quartzdiorites are rich in K, these two rock types may appear as monzonites in the IgClass system. Secondary minerals may again have added to this slight discrepancy.

Unit 11 (2205-2542 m) is seen on both logs and cores as a granodiorite. The layers within this unit are primarily granite and tonalite on the log-based column, and diorite and tonalite on the rock-based column. Unit 12 (2542-2595 m), the major fault zone, has extensive zeolite alteration which caused the silicon content to be high. Therefore, the unit appeared as granite in the IgClass system.

Diorites and monzonites dominate unit 13 (2595-2830 m) on the log-based column, a result similar to the tonalites and diorites with monzongranite gneisses described in the rock. Unit 14 (2830-3103 m) represents a granite-to-monzonite layered with diorite on the log-based column, also seen in the core-based column as monzogranite-to-granodiorite with a layer of diorite in the rocks.

Unit 15 (3103-3335 m) is highly variable on the log-based column, dominated by tonalites, granodiorites, and monzonites; cores and cuttings within this unit are described as tonalite with three, heavily altered fault zones. Unit 16 (3335-3430 m) is also highly variable, dominated by granodiorites with interlayered granitic intervals increasing with depth. The cores within are described as monzogranites, granodiorites, and tonalites.

SUMMARY AND CONCLUSIONS

The oxide abundances from the geochemical logs of the Cajon Pass well compare favorably with oxide measurements from core samples, except for MgO in the upper and Al_2O_3 in the lower parts of the hole. The drilling muds added in the lower portion of the hole badly affected the Al measurement, and the Ca and Ti measurements somewhat less.

The linear regression of log versus core values was applied to the log measurements to calibrate them. This method of calibration corrects the logs for overall affects of mud contamination, tool miscalibration, or processing errors.

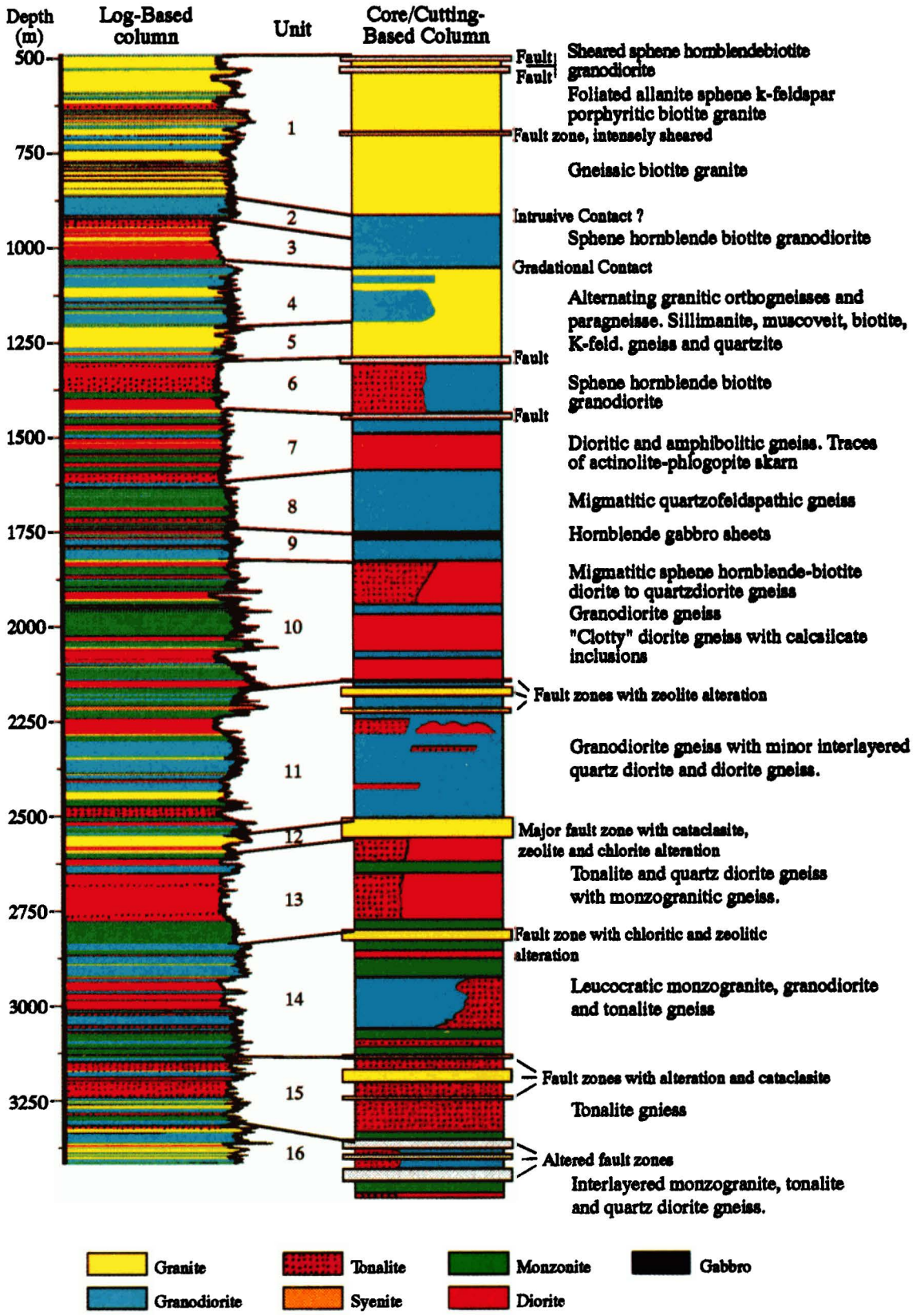

Plate 1. A lithologic column of the Cajon Pass log data as defined by the oxide classification scheme (left) compared to the core/cutting lithologic column (right). The total gamma ray curve was used to form the right-hand margin of the log-based lithologic column. We have divided the Cajon Pass basement into 16 lithologic units, based on the combined log-based and core/cutting-based lithologic columns.

Calibrated results enhance the usefulness of the logs in quantitative applications.

Geochemical logs become more useful when lithology can be determined from them. Because it is often difficult to deduce lithology from elemental and oxide measurements, a new chemical rock classification scheme, IgClass, is presented which incorporates K_2O versus Al_2O_3/SiO_2 to distinguish the major crystalline rock types (syenites, granites, monzonites, granodiorites, diorites, tonalites, and gabbros).

This IgClass system has applications for chemical measurements from either core or log. When applied to geochemical well log measurements, a lithologic column of an entire well in 0.15-m (6 inches) increments can be produced in a matter of hours. A similar undertaking, based on continuous core retrieval and analysis, would be extremely time consuming and cost prohibitive. Applications of the classification system to geochemical well logs are particularly useful when striving to produce a lithologic column with as much vertical resolution and depth refinement as possible. In this respect, the logs are superior to cutting-based or intermittent core recovery-based lithologic columns in terms of resolution and depth refinement.

Because the IgClass system uses chemical input only, its ability to allow any textural classification of crystalline rocks is limited. Future testing of the IgClass system may increase this ability. Incorporating other logs, such as the Formation MicroScanner log, may allow for textural classification. The addition of other elements into the process may refine lithologic boundaries distinction.

The usefulness of the IgClass system has been demonstrated on the geochemical well logs of the Cajon Pass drill hole. The chemical classification scheme worked well throughout much of the well. In zones where the classification deviated from that based on rock samples from the well, it is suspected that mineral alteration or rock types containing accessory minerals caused the discrepancy. Because the accuracy of the IgClass scheme depends on the degree of alteration, further research will be needed to develop a means for subtracting out these secondary alteration and accessory minerals from the chemical measurements. Clearly, the chemical log-based lithologic classification enhances the geologic interpretation of the Cajon Pass drill site by providing a lithologic column with higher resolution and depth accuracy.

Acknowledgments. The first author would like to thank L. Pratson, J. Tivy, W. R. Van Schmus, and F. E. Goff for their input on the manuscript and critical review. M. Herron provided useful input on the ideas of the IgClass system. S. Cotkin contributed to the petrographic cutting and thin-section observation and the petrological classification of the geologic column. Lamont-Doherty Geological Observatory contribution number 4878.

REFERENCES

Anderson, R. N., R. E. Dove, C. Broglia, L. T. Silver, E. W. James, and B. W. Chappell, Elemental and mineralogical analyses using geochemical logs from the Cajon Pass Scientific Drill hole, California, and their preliminary comparison with core analyses, *Geophys. Res. Lett.*,*15*(9), 969-972, 1988.

Anderson, R. N., J.C. Alt, J. Malpas, M. A. Lovell, P. K. Harvey, and E. Lewis Pratson, Geochemical well logging in basalts: The Palisades sill and the oceanic crust of Site 504B, *J. Geophys. Res.*, *95*, 9265-9292, 1990.

Chapman, S., et al., The emergence of geochemical well logging, *Tech. Rev. 35*(2), 27-35, 1987.

Doveton, J., *Log Analysis of Subsurface Geology: Concepts and Computer Methods*, 273 p, Wiley-Interscience, New York, 1986.

Flaum, C., and G. Pirie, Determination of lithology from induced gamma-ray spectroscopy, *Trans. SPWLA Annu. Logging Symp. 24th*, paper H, 1981.

Grau, J. A., and J. S. Schweitzer, Elemental concentrations from thermal neutron capture gamma-ray spectra in geologic formations, *Nucl. Geophys.*, *3*(1), 1-9, 1989.

Herron, M. M., Mineralogy from geochemical well logging, *Clays Clay Miner.*, *34*, 204-213, 1986.

Herron, M. M., Geochemical classification of terrigenous sands and shales from core or log data, *J. Sediment. Petrol.*, *58*(5), 820-829, 1988.

Hertzog, R., et al., Geochemical logging with spectrometry tools, SPE paper 16792 presented at Annual Technical Conference, Soc. of Pet. Eng., Dallas, Tex., 1987.

Jackson, K. C., *Textbook of Lithology*, 552 pp., McGraw-Hill, New York, 1970.

Lachenbruch, A. H., and J. H. Sass, Heat flow and energetics of the San Andreas fault zone, *J. Geophys. Res.*, *85*, 6185-6223, 1980.

Lachenbruch, A. H., and J. H. Sass, The stress heat-flow paradox and thermal results from Cajon Pass, *Geophys. Res. Lett.*, 15(9), 981-984, 1988.

Middleton, G. V., Chemical composition of sandstones, *Geol. Soc. Am. Bull.*, *71*, 1011-1026, 1960.

Nockolds S. R., Average chemical compositions of some igneous rocks, *Geol. Soc. Am. Bull.*, *6*, 1007-1032, 1954.

Pettijon, F. J., P. E. Potter, and R. Siever, *Sand and sandstone*, 618 pp., Springer-Verlag, New York, 1972

Peveraro, R. C. A., and K. J. Russell, Interpretation of wireline log and core data from a mid-Jurassic sand/shale sequence, *Clay Miner.*, *19*, 483-505, 1984.

Scholz, C. H., Shear heating and the state of stress on faults, *J. Geophys. Res.*, *85*, 6174-6184, 1980.

Schweitzer, J. S., D. V. Ellis, J. A. Grau, and R. C. Hertzog, Elemental concetrations from gamma-ray spectoscopy logs, *Nucl. Geophys.*, *2*(3), 175-181, 1988.

Scott, H. D., and M. P. Smith, The aluminum activation tool, *Log Anal.*, *14*(5), 3-12, 1973.

Silver, L. T., E. W. James, and B. W. Chappell, Petrological and geochemical investigation at the Cajon Pass deep drillhole, *Geophys. Res. Lett.*, *15*(9), 961-964, 1988.

Streckeisen, A. L., To each plutonic rock its proper name, *Earth Science Reviews.*, *12*, 1-33 1976.

Wendlandt, R. F., and K. Bhuyan, Estimation of mineralogy and lithology from geochemical log measurements, *Am. Assoc. Pet. Geol. Bull.*, *74*(6), 837-856, 1990.

Zoback, M. D., H. Tsukahara, and S. Hickman, Stress measurements at depth in the vicinity of the San Andreas Fault: Implications for the magnitude of shear stress at depth, *J. Geophys Res.*, *85*, 6157-6173, 1980.

Zoback, M. D., et al., New evidence on the state of stress of the Sand Andreas fault system, *Science*, *238*, 1105-1111, 1987.

R.N. Anderson, M. Lyle, and E.L. Pratson, Borehole Research Group, Lamont-Doherty Geological Observatory, Palisades, NY 10964.

B.W. Chappell, Department of Geology, Australia National University, Canberra, Australia.

R.E. Dove, Schlumberger-Doll Research, Old Quary Road, Ridgefield, CT 06877.

E.W. James, Bureau of Economic Geology, The University of Texas at Austin, University Station, Box X, Austin TX 78713-7508.

L.T. Silver, Department of Geological and Planetary Sciences, California Institute of Technology, Pasadena, CA 91125.

(Received May 20, 1991;
revised October 3, 1991;
accepted October 17, 1991.)